N2O emissions from decomposing crop residues are strongly linked to their initial soluble fraction and early C mineralization

Gwenaëlle Lashermes, Sylvie Recous, Gonzague Alavoine, Baldur Janz, Klaus Butterbach-Bahl, Maria Ernfors, Patricia Laville

N_2O emissions from decomposing crop residues are strongly linked to their initial soluble fraction and early C mineralization

Gwenaëlle Lashermes[a,*], Sylvie Recous[a], Gonzague Alavoine[a], Baldur Janz[b], Klaus Butterbach-Bahl[b], Maria Ernfors[c], Patricia Laville[d]

[a]Université de Reims Champagne Ardenne, INRAE, FARE, UMR A 614, 51097 Reims, France
[b]Karlsruhe Institute of Technology, Institute of Meteorology and Climate Research–Atmospheric Environmental Research, Garmisch-Partenkirchen, Germany
[c]Swedish University of Agricultural Sciences, Department of Biosystems and Technology, P.O. Box 103, SE-230 53 Alnarp, Sweden
[d]Paris-Saclay, INRAE, AgroParisTech, UMR ECOSYS, 78850, Thiverval-Grignon, France

*Corresponding author: INRAE, UMR FARE, 2 Esplanade Roland Garros, 51100, Reims, France. gwenaelle.lashermes@inrae.fr

Keywords
Decomposition
Greenhouse gas (GHG)
Litter
Nitrous oxide
Nitrogen
Soil

Graphical abstract

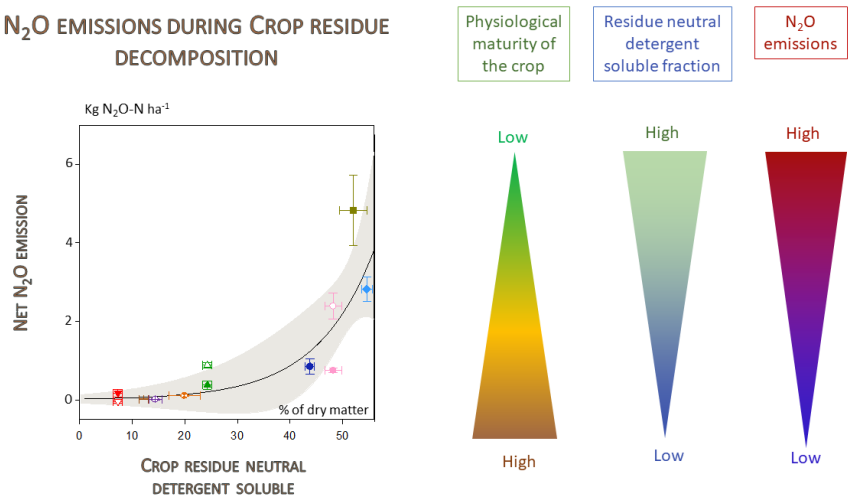

Abstract

The emission of nitrous oxide (N_2O), a strong greenhouse gas, during crop residue decomposition in the soil can offset the benefits of residue recycling. The IPCC inventory considers agricultural N_2O emissions proportional to the amount of nitrogen (N) added by residues to soils. However, N_2O involves several emission pathways driven directly by the form of N returned and indirectly by changes in the soil induced by decomposition. We investigated the decomposition factors related to N_2O emissions under controlled conditions. Residues of sugar beet (SUB), wheat (WHT), rape seed (RAS), potato (POT), pea (PEA), mustard (MUS), red clover (RC), alfalfa (ALF), and miscanthus (MIS), varying by maturity at the time of collection, were incubated in two soils (GRI and SLU) at 15°C with a water-filled pore space of 60%. The residues contained a wide proportion range of water-soluble components, components soluble in neutral detergent (SOL-NDS), hemicellulose, cellulose, and lignin. Their composition drastically influenced the dynamics of C mineralization and soil ammonium and nitrate and was correlated with N_2O flux dynamics. The net cumulative N_2O emitted after 60 days originated mostly from MUS (4828 ± 892 g N-N_2O ha^{-1}), SB (2818 ± 314 g N-N_2O ha^{-1}) and RC (2567 ± 1245 g N-N_2O ha^{-1}); the other residue treatments had much lower emissions (<200 g N-N_2O ha^{-1}). For the first time N_2O emissions could be explained only by the residue content in the SOL-NDS, according to an exponential relationship. Residues with a high SOL-NDS (>25% DM) were also non-senescent and promoted high N_2O emissions (representing 1–5% of applied N), likely directly by nitrification and indirectly by denitrification in microbial hotspots. Crop residue quality appears to be valuable information for accurately predicting N_2O emissions and objectively weighing their other potential benefits to agriculture and the environment.

Highlights

- N_2O emissions were measured during laboratory incubations of soil and crop residues
- The coupling of N_2O and CO_2 emissions and soil mineral N dynamics was studied
- Nine crop residues whose compositions widely varied were incubated in two soils
- The residue neutral detergent soluble content explained the observed N_2O emissions
- The IPCC could underestimate the N_2O emissions of residues from nonsenescent crops

1. Introduction

The recycling of crop residues into the soil is an important mechanism for increasing the sequestration of carbon (C) in the soil; additionally it contributes to the mitigation of greenhouse gases (GHGs) in the atmosphere (*cf.* the "4 per 1000" initiative, Minasny et al., 2017) and aids in the maintenance of the organic matter levels in the soil, reducing the risk of erosion and promoting food safety (FAO, 2017). However, GHG nitrous oxide (N_2O), whose potential to exacerbate global warming is 265 times greater than that of carbon dioxide (CO_2), is emitted during crop residue decomposition. Assessments of the GHG balance of cropping systems have shown that the N_2O emissions associated with crop residue decomposition can, in some situations, offset the positive effects that the recycling of crop residues has on maintaining or increasing soil C stocks (Li et al., 2005; Lugato et al., 2018; Xia et al., 2018). The methods used to inventory GHG emissions from the agricultural sector account for the impact of crop residues in the same way that organic amendments or synthetic fertilizers are accounted for through the amount of nitrogen (N) they add to soils. To account for N_2O emissions from added residue N, an emission factor was assigned; this factor was recently revalued and found to be 0.006 N_2O-N kg^{-1} N returned in wet climates and 0.005 N_2O-N kg^{-1} N returned in dry climates (Hergoualc'h et al., 2019). This implies that the chemical (other than N) characteristics of the residues and the agricultural practices applied to them (e.g., whether they are buried) are not considered. Due to the lack of data and the sometimes conflicting results on the effects of residues on N_2O emissions, several recent studies and syntheses have attempted to identify the determinants of emissions associated with the recycling of plant biomass and to determine the emission factors (e.g., Butterbach-Bahl et al., 2013; Chen et al., 2013; Xia et al., 2018; Schmatz et al., 2020).

N_2O is produced by several pathways, mainly during nitrification and denitrification. N_2O production, consumption and emissions depend on various physicochemical and microbial parameters, such as the quantity and forms of mineral N available, heterotrophic microbial activity, the presence of communities of specific autotrophic microbes, oxygenation conditions, temperature, humidity, and the presence of reactants (Butterbach-Bahl et al., 2013). Unlike N added via mineral fertilizer, the N supplied via organic substrates such as crop residues impacts a series of concomitant processes. Indeed, organic substrates quickly and significantly affect the heterotrophic microbial growth of decomposers and their demand for oxygen and nutrients and the ammonification and microbial N assimilation fluxes at equilibrium, on which the availability of mineral N depends (Mary et al., 1996; Zhao et al., 2018). Depending on whether they are deeply or superficially buried or left as mulch on the soil surface, residues also impact the physical properties of soil, such as soil aggregation and soil water content (Le Guillou et al., 2012). Therefore, aside from a possible direct effect of N addition via crop residue on N_2O emissions, the presence and decomposition of crop residue first act as indirect factors that affect N_2O emissions, and the magnitude of this indirect effect depends on other characteristics, particularly their chemical composition and biodegradability. Recent studies have revealed that there is a close relationship between CO_2 and N_2O fluxes during the decomposition of crop residues, which emphasizes the role of the chemical composition of residues and their degradation kinetics as drivers of N_2O emission-generating processes (Schmatz et al., 2020; Surey et al., 2020). However, the effects of the crop residue composition and the resulting interactions among decomposition kinetics, N dynamics and N_2O emissions have hardly been explored, as most relevant studies have characterized residues only by their N content or by their C:N ratio (Zhao et al., 2018; Chen et al., 2013).

As such, the aim of this work was to understand how N_2O emissions are influenced by crop residue characteristics during their decomposition in the soil and whether the residue C and N characteristics affect the dynamics and intensity of N_2O fluxes. To accomplish this aim, we performed experiments with nine different crop species residues that are representative of agriculture in temperate conditions and two soils under controlled conditions. We assessed the initial chemical composition of the residues and in high temporal resolution the dynamics of C mineralization and the content of both the ammoniacal (NH_4^+) and nitric (NO_3^-) mineral forms in the soil in parallel with N_2O emissions. Three of the nine residues were incubated in another soil to examine the relative influence of the soil type. The chemical compositions of the nine crop residues varying by agricultural use were characterized via the different chemical criteria that influence the decomposition dynamics, and their propensity for and intensity of N_2O fluxes were evaluated. We used an experimental approach with repacked soil cylinders and calibrated residues. Although we are aware that this design is a

simplified and standardized representation of residue decomposition in soil in the context of agriculture, this approach allows us to assess the role of the characteristics of crop residues while minimizing the confounding effects that would occur under field conditions, such as climate, spatial variability, type of crop, residue localization, and soil heterogeneity.

2. Materials and methods

2.1. Sites, soils, and preparation

The two soils used for experiments were collected in spring 2018 and included soil from the 0–20 cm tilled layer at the experimental station of the French National Research Institute for Agriculture, Food and Environment (INRAE) in Thiverval-Grignon, France (GRI soil) (latitude 48°50'58.5"N, longitude 1°56'04.3"E) and soil from at the experimental station of the Swedish University of Agricultural Sciences (SLU) at the Lönnstorp field, in Åkarp, Sweden (SLU soil) (latitude 55°39'58.5"N, longitude 13°06'57.1"E) (Table S1). The GRI soil is an alkaline calcareous silty clay loam under annual crop rotation and was sampled from under winter wheat (WHT) (*Triticum aestivum*). The organic C, total N, clay, silt, sand, and $CaCO_3$ contents were 18.4, 1.79, 214, 358, 147, and 275 g kg^{-1} dry soil, respectively. The SLU soil is a slightly acidic sandy loam and was sampled from a field growing sugar beet (SUB) (*Beta vulgaris* L.); no cover crop was grown during winter of the previous year in this field. The organic C, total N, clay, silt, sand, and $CaCO_3$ contents were 15, 1.49, 158, 224, 618, and <0.1 g kg^{-1} dry soil, respectively. The C:N ratios of the two soils were similar (10), while the pH (H_2O) values were 8.3 and 6.2, respectively, and the cation exchange capacity (CEC) values were 13.6 and 10.5 cmol+ kg^{-1} dry soil for the GRI and SLU soils, respectively. Visible plant residues were removed from the soil. The fresh soil was then air dried to approximately 0.15 g H_2O g^{-1} dry weight (DW), sieved to < 6 mm, and subsampled to analyze the texture, total C content, total N content, and pH. The GRI soil was stored at < 4°C to limit microbial activity, while the SLU soil was frozen at –20°C for shipment from Sweden to France. The SLU soil was thawed in air at room temperature one day before sieving, and both soils were preincubated for one week at 15°C at a water content of 200 g kg^{-1} dry soil and a density of 1.0 g cm^{-3}. At the beginning of the experiment, the residues were remoistened to a moisture content of 20 or 80 g 100 g^{-1} dry matter (DM) (Table 2), reflecting the actual moisture content of these residues in the field when they return to the soil (Thiébeau et al., 2021). The deionized water added corresponded to 0.14 g g^{-1} DM for the miscanthus (MIS), WHT, rape seed (RAS), pea (PEA), and potato (POT) residues and to 3.92 g g^{-1} DM for the other residues. All the residues were allowed to absorb water for 10 to 15 min before being added to the soil samples.

A soil water retention curve for each of the two soils (gravimetric water content [ϑ] *vs*. water potential [ψ]) was constructed on the basis of Richards' press method (Klute, 1986), in which 5 bar and 15 bar pressure plate extractors (Soil Moisture Equipment Corp., Santa Barbara, California, USA) were used. The applied ψ varied from -1500 to -5 kPa (*i.e.*, pF 4.2 to 1.7), and the corresponding ϑ of the soil aggregates varied from 128.3 to 405.9 g kg^{-1} dry soil for the GRI soil and from 85.5 to 305.3 g kg^{-1} dry soil for the SLU soil (Table S1, Supplementary Material [SM]).

2.2. Crop residue and chemical measurements

Shoots of nine plant species from 5 botanical families (*Amaranthaceae*, *Brassicaceae*, *Fabaceae*, *Poaceae*, *Solanaceae*) were selected for the experiment: MIS, WHT, RAS, PEA, alfalfa (ALF), POT, red clover (RC), mustard (MUS), and SUB (Table 2). This range of residues encompasses five agricultural uses (main crop, cover crop, crop dedicated to energy production, hay, and market gardening) and covers three stages of plant maturity at the time of harvesting (green, maturity, and senescence). The proportions of the different plant organs (leaves, stems, ramifications, *etc.*) were standardized for each residue in proportions similar to those that occur in the field, and the residues were cut by hand into small pieces 1 cm in length. The RC was obtained from a field experiment at the Norwegian University of Life Sciences (NMBU) in Børsum, Norway (latitude 59° 39' 45"N, longitude 10° 45' 46"E). The RC residue was dried for one week at 40°C. ALF residue was obtained from a 3-year alfalfa crop sampled just before mowing at the end of June 2018 from the experimental site of the agricultural secondary school in Somme-Vesle, France (49°00'41.9"N 4°35'15.2"E). Only the first 10 cm of each of the plant (collar) and shoot litter samples that was slated to return to soil were retained. Other residues were obtained from the INRAE experimental site of Estrées-Mons (49°52'23.88'' N 3°1'53.04'' E) in July 2017. The residues were dried at 35°C for one week to remove senescent residues and for two weeks to remove green

residues before storage and chemical determination. The residue moisture content was determined by drying subsamples at 80°C for 24 h.

The chemical characteristics of each residue were determined. The residues were ground to 80 µm pieces to determine the total C and N contents by elemental analysis (Euro-EA, Eurovector, Milan, Italy), with the residue water-soluble C (WSC) and N (WSN) determined by water extraction (water:residue, 200:1 [v/w], 30 min, 20°C), expressed in grams of C per 100 grams of DM and gram of N per 100 grams of DM, respectively. The WSC content of the extracts was analyzed using an autoanalyzer (Aurora Model 1030, O.I. Analytical, College Station, TX, USA). The WSN content was determined by dry combustion according to the standard NF EN 12260 protocol (AFNOR, 2004), and the residue NH_4^+-N and NO_3^--N contents were measured by continuous flow colorimetry in water extract, expressed in grams of N per 100 g of DM. The chemical composition was then determined by proximate analysis (Goering and Van Soest, 1970). For this, in the first step, the fraction soluble in neutral detergent (SOL-NDS) was extracted from 1 mm ground litter samples in hot water (30 min, 100°C) and then in neutral detergent (1 h, 100°C). Afterward, the remaining residual after SOL-NDS extraction was successively extracted with dilution and acid to extract the hemicellulose fraction (HEM), cellulose fraction (CEL) and lignin fraction + ash (LIG), expressed in grams per 100 grams of DM.

2.3. Incubation experiments

2.3.1. Experimental setup

The experiment involved incubation for 60 days in the dark at 15 ± 1°C to measure the C mineralization, soil mineral N dynamics and N_2O emissions. The 14 treatments consisted of nonamended soils (as controls) and soil + residues for the 9 crop species and 2 soils listed above (Table 1, Table S1). The treatments were arranged in a completely randomized design, and each treatment was replicated three times. Moist residue particles were added at a rate equivalent to 8.3 g DM kg^{-1} of dry soil in the amended treatments (equivalent to the incorporation of 4.0 Mg DM ha^{-1}. The targeted water-filled pore space (WFPS) was 60% (i.e., 60 cm^3 of water cm^{-3} of soil porosity) throughout the incubation and was maintained by the addition of distilled water when necessary. The corresponding soil ϑ was 254 g kg^{-1} dry soil, calculated as follows (Linn and Doran, 1984):

$$\theta = \frac{WFPS \cdot n}{\rho_t}, \text{ with } \quad n = 1 - \frac{\rho_t}{\rho_s} \qquad (1)$$

where ρ_t is the bulk density in grams per cubic center, n is the porosity in cubic centimeters per cubic centimeter, and ρ_s is the particle density (using the standard default value of 2.65 g cm^{-3}). The corresponding soil ψ values were pF 2.5 for the GRI soil and pF 1.9 for the SLU soil, which were approximately 15% and 62% greater, respectively, than their moisture at field capacity.

Incubation was performed in acrylic cylinders (7.0 cm in diameter and 10.0 cm in height) containing soil cores 8 cm in height. First, for each residue-amended replicate, a subsample of 244 g of moist soil was placed in the cylinder and gently squeezed until a height of 4 cm was reached. Afterward, a second subsample consisting of a mixture of 244 g of moist soil and residue particles was placed in the same acrylic cylinder and compressed such that the total height was 8 cm. Thus, the soil in each pot had a final moist soil weight of 488 g and a bulk density of 1.25 g cm^{-3}. The cylinders were subsequently placed in a glass jar that had a volume of 3 L that was hermetically closed to prevent drying but periodically opened to maintain aerobic conditions. A series of cylinders were prepared in parallel in the same way for the different measurements (CO_2, mineral N, and N_2O). An exception was for the samples dedicated to N_2O emission measurements, which were prepared slightly differently to fit the N_2O emission measuring device; i.e., these soil cylinders were 7.4 cm in diameter and 10.0 cm in height, and the total weight was 539 g moist soil.

The moisture measurements showed that the WFPS averaged 60% for the control soils, varying between 58 and 61% for the GRI soil and between 56 and 63% for SLU soil (data not shown). Since residues provide some water, the WFPS averaged 61% for the soil and residue treatments. Initially, the wet soil sample was homogeneous, then a slight gradient formed over time, the WFPS was slightly lower in the 0–4 cm soil layer than in the 4–8 cm soil layer for the control soils (on average 57% and 63%, respectively at the end of incubation), and a slight reverse gradient was observed for the soils with residues (on average, a WFPS of 63% in the 0–4 cm soil layer with the residue and 60% in the 4–8 cm soil layer), which gradually disappeared. The whole incubation process was split into two incubation periods to decrease the number of jars and samples simultaneously in use. The SUB, WHT, RAS, RC, POT, PEA, and MUS residues were incubated in GRI soil during the first incubation.

Table 1. Crop residues used for incubation and their stage of maturity, initial moisture content and chemical composition (means ± standard errors)

Common name	**Miscanthus (MIS)**	**Wheat (WHT)**	**Rape seed (RAS)**	**Pea (PEA)**	**Alfalfa (ALF)**	**Potato (POT)**	**Red clover (RC)**	**Mustard (MUS)**	**Sugar beet (SUB)**
Binomial nomenclature	*Miscanthus x giganteus*	*Triticum aestivum*	*Brassica napus oleifera*	*Pisum arvense*	*Medicago sativa*	*Solanum tuberosum*	*Trifolium pratense*	*Sinapis arvensis*	*Beta vulgaris*
Family	Poaceae	Poaceae	Brassicaceae	Fabaceae	Fabaceae	Solanaceae	Fabaceae	Brassicaceae	Amaranthaceae
Plant organ of the mixture[a]	senescent leaves (100)	stems (50), leaves (50)	main stems (42), stem ramifications (27), inflorescences (31)	milled leaves and stems (100)	collars (66), senescent collars (13), soil litter (21)	stems (27), leaves (73)	stems (27), leaves and inflorescences (34), petioles (29)	stems (64), green leaves (34), senescent leaves (2)	stems (26), green leaves (37), senescent leaves (5), collar (32)
Maturity stage at the time of harvest	senescence	senescence	senescence	senescence	green stage	physiological maturity	green stage	green stage	physiological maturity
Initial residue Moisture content[b]	20	20	20	20	80	20	80	80	80
Plant use	energy crop	main crop	main crop	main crop	main crop	market gardening	hay	cover crop	main crop
Total C[a]	46.2 ± 0.3	46.6 ± 0.1	45.3 ± 0.4	45.3 ± 0.2	46.4 ± 0.4	41.1 ± 0.5	44.5 ± 0.1	41.9 ± 0.3	38.9 ± 0.4
Total N[a]	0.4 ± 0.0	0.5 ± 0.0	0.5 ± 0.0	1.0 ± 0.0	1.4 ± 0.0	3.4 ± 0.0	2.5 ± 0.0	2.6 ± 0.0	2.4 ± 0.0
Total C:N	128	91	99	43	34	12	18	16	16
WSC:WSN	28	24	16	18	24	10	38	22	23
NO_3^--N[c]	0.1 ± 0.0	0.4 ± 0.2	6.9 ± 0.5	2.2 ± 0.5	1.2 ± 0.4	79.5 ± 27.0	0.2 ± 0.2	3.3 ± 1.1	11.1 ± 0.7

WSC, water-soluble C; WSN, water-soluble N; [a] percentage of dry matter; [b] percentage of wet weight; [c] g g^{-1} dry matter

The ALF and MIS residues were incubated in GRI and SLU soils during the second incubation, and RC residues were incubated in SLU soil. These cross-incubations in the two soils were applied to analyze the effects of the soil on residue-derived N_2O emissions. The initial soil NO_3^--N and NH_4^+-N contents slightly differed between the two incubations as follow: the contents were 23.7 and 0.5 mg kg^{-1} dry soil, respectively, for the GRI soil for the first incubation; 26.5 and 0.6 mg kg^{-1} dry soil, respectively, for the GRI soil for the second incubation; and 21.9 and 0.5 mg kg^{-1} dry soil, respectively, for the SLU soil for the second incubation.

2.3.2. Mineral N contents

The mineral N contents of the top and bottom soil layers were determined in all treatments at time 0 and after 7, 14, 28 and 60 days of incubation. At each sampling time, a subsample of 50 g from each layer was carefully removed and immediately frozen to enable the standardization of the process timing for all the residue types and their replicates on each date and between dates (Sterckeman and Ciesielski, 1991). Mineral N was later extracted from the freshly thawed soils with 200 mL of 1 M KCl (soil:solution, 1:4, 30 min of shaking). The supernatants were frozen until analysis. Their mineral N contents were determined by continuous flow colorimetry using an autoanalyzer (TRAACS 2000, Bran and Luebbe, Norderstedt, Germany) according to the method proposed by Kamphake et al. (1967) for NO_3^- determination and the method described by Krom (1980) for NH_4^+ determination. The results are expressed in kilograms of NO_3^--N and kilograms of NH_4^+-N per hectare in each layer.

2.3.3. C mineralization

C mineralization was measured by quantifying the CO_2 release. The CO_2 produced was trapped in sodium hydroxide (NaOH) under excess conditions of CO_2 capture, i.e., 40 mL of 1 M NaOH in a beaker placed inside each 3 L glass jar that was hermetically closed but periodically opened to maintain aerobic conditions (Alavoine et al., 2008). The NaOH beakers were changed at each sampling time, i.e., after 3, 7, 14, 21, 28, 35 and 42 days of incubation. Their carbonate contents were measured by continuous flow colorimetry (Alavoine and Nicolardot, 2002) using an autoanalyzer (TRAACS 2000). C mineralization rates were calculated for the time interval between two sampling times and are expressed in kilograms C-CO_2 per hectare per day. The cumulative C mineralization was calculated as the sum of C-CO_2 evolved during each sampling interval and was expressed in kilograms C-CO_2 per hectare. The conversion of the mineralization rate expressed on a soil-area basis to a soil-weight basis and *vice versa* was performed using the soil core density and height used in this experiment. Indeed, the rates and amounts of C-CO_2 expressed in kilograms per hectare are equivalent to milligrams per kilogram soil. The net residue C mineralization was calculated as the difference in the amount of CO_2-C evolved from each residue-amended treatment and from the corresponding control treatment (so-called apparent mineralization). As such, it is assumed that the mineralization of native soil organic C was not affected significantly by the addition of residue (no priming effect) or that the priming effect was of the same order of magnitude for each of the different residues and did not bias the interpretation regarding the biodegradability of the plant litter studied.

2.3.4. N_2O emissions

N_2O emissions were measured using an integrated mesocosm for N_2O in agriculture (IMNOA) automatic monitoring device that measures headspace N_2O concentrations on the basis of infrared spectrometry (Laville et al., 2019). The N_2O flux was measured 26 times during the incubation period, 5 times $week^{-1}$ during the first 3 weeks, and 11 times in total for the following 5 weeks. Briefly, the acrylic cylinders were placed in a glass jar with a volume of 0.8 L in a climate cabinet with a controlled temperature. Each jar lid was fitted with 2 tubes connected to a 12-port electrodistributor system to measure the distribution of air between the jar and gas analyzer via a data logger (CR1000, Campbell Scientific, Loughborough, UK). The duration of the measurement for each jar was 10 min and included the 3 phases, which allowed evaluation of the fluxes by two methods, i.e. the "open jar" or "closed jar" methods. The use of two additional electrodistributors made it possible to manage the different phases. During the first phase, the outside air circulated in the jar and was measured until a steady-state concentration was reached. In the second phase (3 min), the same jar was isolated (the biogas accumulated in the jar), and the outside concentration was measured. During the third phase, the air circulated again in the jar, and the maximum concentration resulting from gas accumulation during the previous phase was evaluated just after the valve was activated. The N_2O concentration was monitored continuously every 1 s using an infrared spectrometer

(QC-TILDAS, Aerodyne Research, MA, USA). In addition to the main measuring circuit, an auxiliary circuit was used to maintain the gas in the nonmeasured jars at a concentration close to the concentration outside the jars during the two hours of measurement. The mixing ratio of N_2O was corrected for water vapor dilution and broadening effects (Harazono et al., 2015; Deng et al., 2017). Throughout the incubation process, the soil cores were kept in their jar and ventilated with air from the outside through the holes to which the tubes were connected.

The N_2O fluxes were measured using two methods and were calculated using two equations. For the open jars, the equation employed was as follows:

$$F_{ss} = \frac{Q}{A} \cdot (C_{ss} - C_{out}). \quad (2)$$

For the closed jar, the equation employed was as follows:

$$F_{ac} = \frac{V}{A} \cdot \frac{C_{ac} - C_{ss}}{\Delta t} \quad (3)$$

where Q is the flow rate in the jar (1 L min^{-1}), A is the soil core area (43 cm²), V is the volume of the jar headspace (0.45 L), C_{ss} is the steady-state concentration after 6 min of flushing, C_{out} is the outside concentration, and C_{ac} is the concentration measured after gas accumulation during the Δt period (180 s).

The fluxes were estimated mainly by the open jar method. The N_2O fluxes corresponded to instantaneous rates at the time of measurement, expressed in grams of N-NO_2 per hectare per day. The cumulative N_2O emissions on day d_j and $CumN_2O_{d_j}$, expressed in grams of N-NO_2 per hectare, were calculated based on linear interpolation between measurement times j and $j-1$ using the following equation:

$$CumN_2O_{d_j} = CumN_2O_{d_{j-1}} + \frac{FN_2O_{d_j} + FN_2O_{d_{j-1}}}{2} \cdot \frac{1}{d_j - d_{j-1}} \quad (4)$$

where $FN_2O_{d_j}$ is the N_2O flux measured on day d_j. The net residue N_2O emissions were calculated as the difference between each residue-amended treatment and the control treatment.

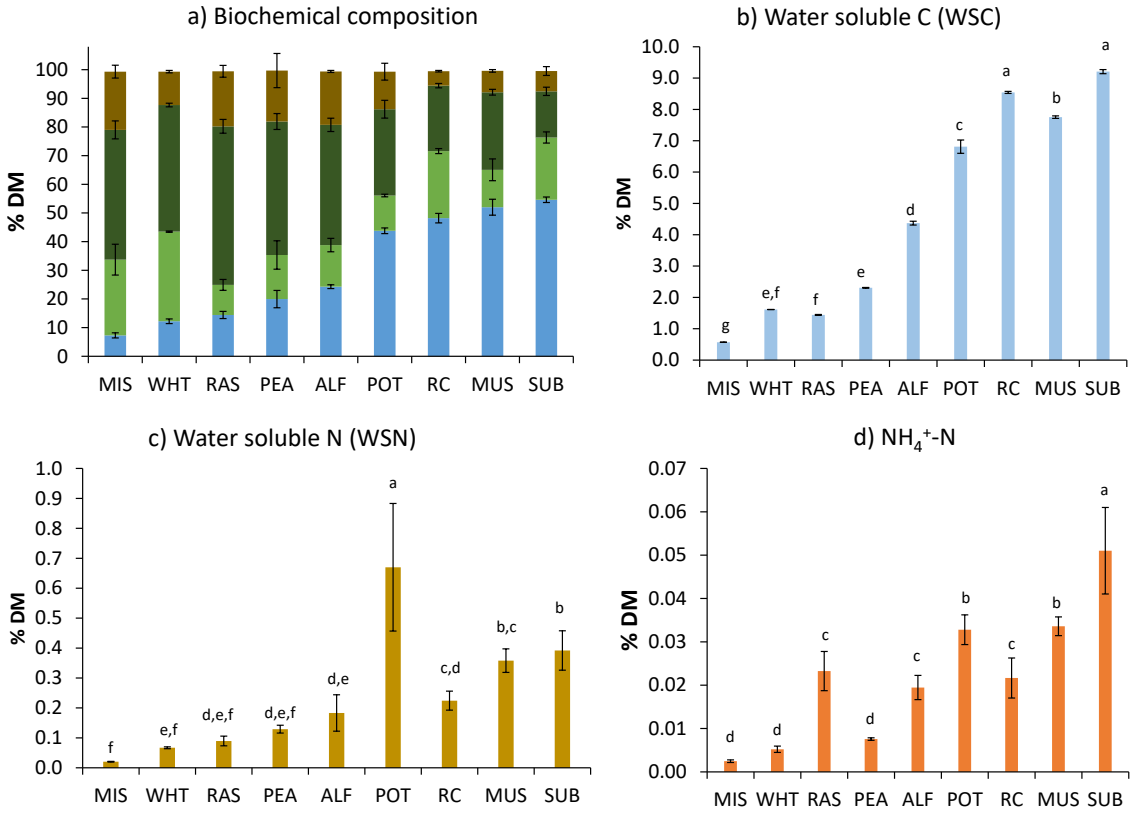

Figure 1. a) Initial biochemical composition of crop residues, as determined according to the van Soest procedure, and the b) WSC, c) WSN, and d) NH_4^+-N contents expressed as a percentage of DM. The biochemical composition includes the SOL-NDS, HEM, CEL and LIG fractions. For the residue abbreviations, see Table 2. The values represent the means ± SEs of three replications. Significant differences among the treatments were tested through one-way ANOVA for b and c (n=27, significance level $P < 0.05$, Benjamini and Hochberg correction for P-values). The different letters indicate significant differences among the treatments (Tukey's HSD test, α=0.05).

The N_2O emission factor (*EF*-N_2O) was calculated as the difference between the raw cumulative emissions from the treatment $CumN_2O_{treatment}$ and the soil control $CumN_2O_{control}$, expressed as a percentage of the residue N added, in kilograms of N per hectare.

$$EF - N_2O = 100 \cdot \frac{CumN_2O_{treatment} - CumN_2O_{control}}{Residue\ N} \quad (5)$$

2.4. Statistics

The results are presented as the means and standard errors of the mesocosm replications for each soil and residue treatment. The initial residue characteristics were compared using one-way ANOVA and Tukey's honestly significant difference (HSD) (α = 0.05) tests. The net cumulative CO_2 and N_2O emissions at the end of incubation, the net CO_2 and N_2O emission rates, and *EF*-N_2O for the soil and residue treatments were compared using one-way ANOVA and Tukey's HSD (α = 0.05) tests performed with XLSTAT-Ecology software (version 18.2, Addinsoft, Paris, France). To avoid false positives related to multiple testing, we corrected all of the P-values via Benjamini and Hochberg false discovery rate control (Verhoeven et al., 2005). Principal component analysis (PCA) was performed to provide an overview and analysis of the relationships between the initial soil mineral N content, the mean initial residue chemical composition properties, the early C and N mineralization in the soil, and the N_2O emissions after 7 and 60 days. The initial residue moisture content was considered a class variable (wet *vs.* dry) and was used as an illustrative variable in the analysis. PCA allows multicollinearity analysis of datasets and was used to extract and summarize important information from the principal component data. All of the data were checked for normality and transformed to meet the requirements before analysis. Based on the first 5 components that explained more than 95% of the observed variability, agglomerative hierarchical clustering (AHC) was carried out using the Ward algorithm to cluster the most comparable soil and residue treatments together (n=2, 3, and 4). The linear relationships between the net cumulative N_2O emissions on day 60 and the initial residue characteristics were tested using the best subsets procedure of SigmaPlot software (version 12.0, Systat Software, Palo Alto, CA, USA). This procedure helped identify useful predictors among the initial residue characteristics by assessing all possible models and displaying the best adjusted coefficient of determination (r_a^2) and Mallow C_P values for each subset of 1 to all the variables. The nonlinear relationships with net cumulative N_2O emissions on day 60 were further investigated with the initial residue characteristics from the best subset variables (the SOL-NDS content, WSC content, total C:N, NO_3^{+-}N content, and WSN content). Exponential growth regression with coefficients of 1, 2, and 3 (or exponential decay for total C:N) was performed using the "dynamic fitting" procedure of SigmaPlot. The goodness of fit of the regression equations was evaluated through the coefficient of determination (r^2) and r^2_a.

3. Results

3.1. Crop residue characteristics

Residue N mainly consisted of the organic form in all residues (> 93.2 ± 0.4% of total N), with the exceptions of the POT residue, which had a significantly higher NO_3^--N content than those of the other residues (statistics not shown) and a high NH_4^+-N content (Table 1, Fig. 1d), and the RAS residue, whose total N comprised 15±1% and 5±1% of mineral NO_3^--N and NH_4^+-N forms, respectively. The POT, SUB, MUS, and RC residues had the highest WSN contents, which were significant (Fig. 1b). For these residues, the WSC and SOL-NDS contents were higher than 6.8±0.6 and 43.9±2.6% DM, respectively, and were significantly higher than those of the other residues (Fig. 1a, Table S1). The biochemical fractions varied significantly among the residues, with more than 44.2±0.6% DM constituting the CEL for senescent residues (MIS, WHT, RAS, and PEA). Compared with the other residues, the MIS, RAS, PEA, and ALF residues also had significantly higher LIG contents.

3.2. CO_2 respiration

The mean rates of CO_2 respiration of the control soils were not significantly different—4 ± 2 and 3 ± 1 kg C-CO_2 ha^{-1} day^{-1} for the GRI soil in the first and second incubations, respectively, and 4 ± 2 kg C-CO_2 ha^{-1} day^{-1} for the SLU soil (Fig. S1, SM). As expected, C-CO_2 evolved from the residue-amended soils, and the evolution rate was significantly higher than that of their respective control soils. The residue C mineralization kinetics, which were possibly altered by the priming effect, differed significantly between the crop residue treatments.

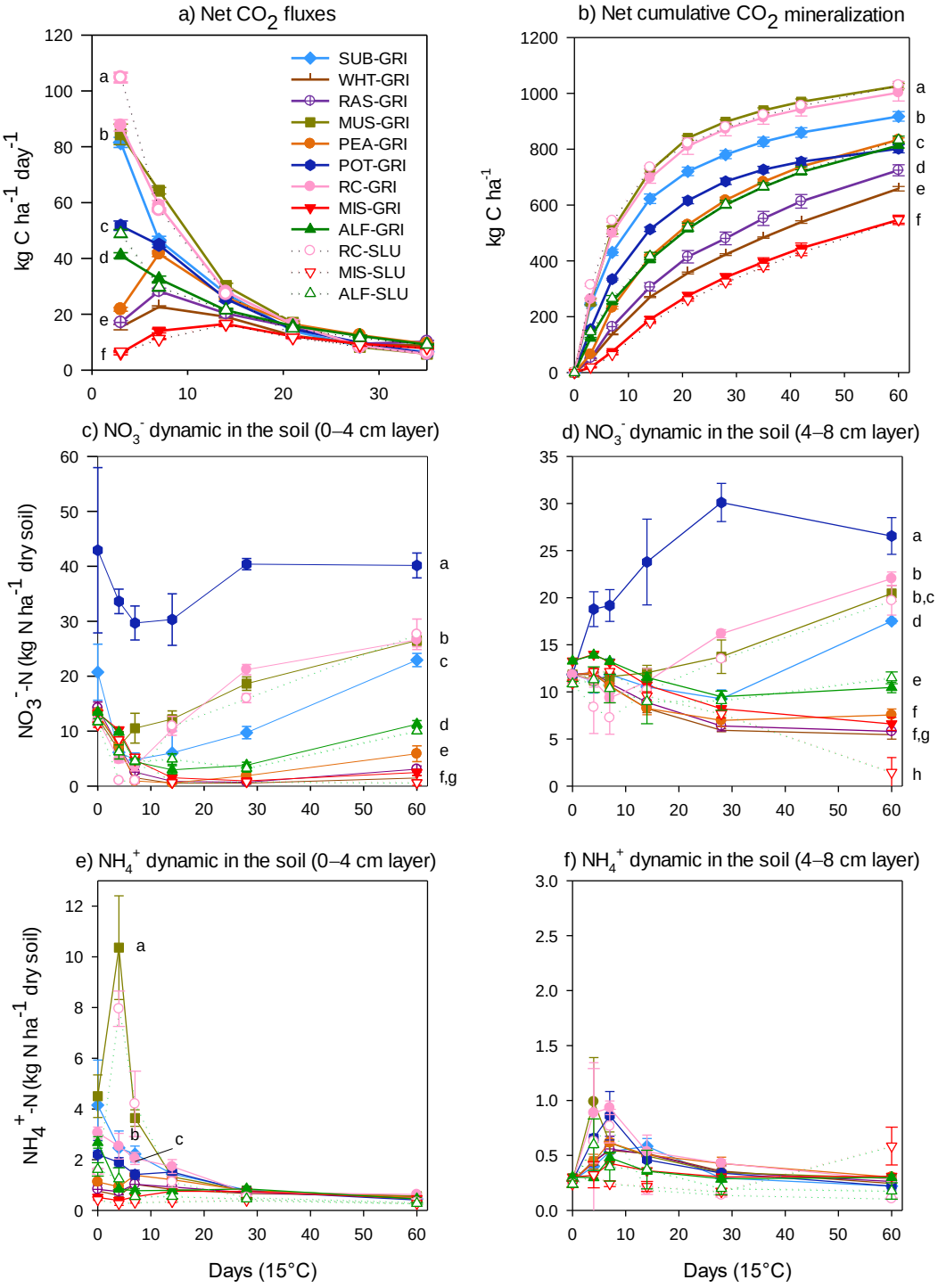

Figure 2. C mineralization and mineral N dynamics in the soil: a) net C mineralization rates, b) net cumulative C mineralization, c) NO_3^--N within the 0–4 cm layer, d) NO_3^--N within the 4–8 cm layer, e) NH_4^+-N within the 0–4 cm layer, and f) NH_4^+-N within the 4–8 cm layer during a 60-day incubation at 15°C with the crop residues incubated in GRI and SLU soils. For the residue abbreviations, see Table 2. The results are expressed per unit of mesocosm surface. The values represent the means of three replicated mesocosms ± SEs. Significant differences among the treatments tested through one-way ANOVA at the end of incubation (a, c, d) at 3 days (b) and at day 7 (e) are indicated (n=36, significance level $P < 0.001$ for a and b, and $P < 0.05$ for c, d, and e, Benjamini and Hochberg correction for P-values). The different letters indicate significant differences among the treatments (Tukey's HSD test, $\alpha=0.01$ for a and b, and $\alpha=0.05$ for c, d, and e).

During the first 0–3-day interval, high rates of mineralization were observed for the RC, MUS and SUB residues in the GRI soil, and the rates decreased continuously until the end of the experiment (Fig. 2a). Significantly lower rates of C mineralization were observed for the POT and ALF residues, but the values were significantly higher than those of the WHT, PEA and RAS residues, while the rate of C-CO_2 evolution was the lowest for the MIS residue. For the WHT, PEA, RAS, and MIS residue treatments, the maximum rates were delayed to the second (3–7) or third (7–14) intervals. Soil type (GRI *vs*. SLU) did not have any effect on either the intensity or dynamics of the MIS, ALF or RC mineralization rates, except for the RC and ALF treatments during the first 0–3-day interval ($P < 0.001$).

As a consequence, the cumulative emissions differed significantly between crop residue treatments (Fig. 2b). During the 60 days of incubation, the MIS and RC residue treatments exhibited similar emissions (equal to 61–59% of the added C), and the emissions of the PEA, POT and ALF residue treatments were intermediate (equal to 44–49% of the added C). The other residues had relatively low C mineralization, i.e., the mineralization proportion in the RAS, WHT, and MIS residue treatments were equal to 40%, 35% and 30% of the carbon added. As expected from the fluxes, there were no significant differences in the cumulative CO_2 respiration under the MIS, ALF, and RC treatments in the GRI and SLU soils.

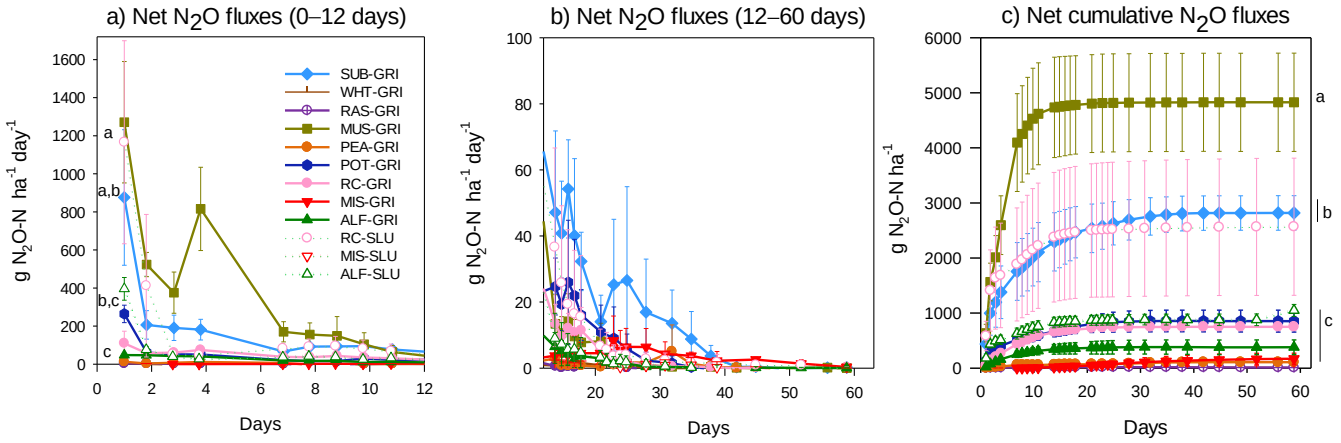

Figure 3. Net N_2O emission rates during a) 0–12 days, b) 12–60 days and c) net cumulative N_2O emissions through incubation when the crop residues were incubated at 15°C in GRI and SLU soils. For the residue abbreviations, see Table 2. The results are expressed per unit of mesocosm surface. The values represent the means of three mesocosm replications ± SEs. Significant differences among the treatments, tested through one-way ANOVA at the end of incubation (a) and 1 day (b), are indicated (n=38, significance level $P < 0.05$, Benjamini and Hochberg correction for P-values). The different letters indicate significant differences among the treatments (Tukey's HSD test, α=0.05).

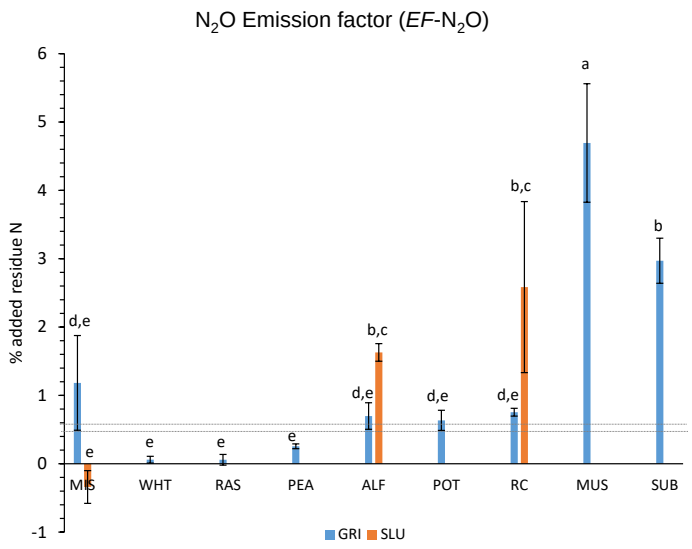

Figure 4. *EF*-N_2O associated with residue decomposition. The values were calculated for cumulative N_2O emissions and are expressed as the percentage of residue N. The values represent the means of three mesocosm replications ± SEs. Emission factors of 0.5% and 0.6% of residue N considered for crop residues in dry and wet climates, respectively, by the IPCC method are visualized by the gray dashed lines. Significant differences among the treatments were tested through one-way ANOVA (n=38, significance level $P < 0.05$, Benjamini and Hochberg correction for P-values). The different letters indicate significant differences among the treatments (Tukey's HSD test, α=0.05).

3.3. Soil NO_3^- and NH_4^+ dynamics

NO_3^- constantly accumulated in the control soils at mean rates of 0.09 ± 0.02 and 0.06 ± 0.02 kg NO_3^--N ha^{-1} day^{-1} for the GRI soil in the first and second incubations, respectively, and at a mean rate of 0.12 ± 0.03 kg NO_3^--N ha^{-1} day^{-1} for the SLU soil (data not shown). Residue addition to the 0–4 cm soil layer induced a marked decrease in the NO_3^--N content in this layer by day 4 for the RC-SLU, RC-GRI, SUB-GRI, and RAS-GRI treatments (Fig. 2c). For all the treatments except the MUS-GRI and POT-GRI treatments, the NO_3^--N fell below 5 kg NO_3^--N ha^{-1} (i.e., 5 mg NO_3^--N kg^{-1} dry soil). The NO_3^--N content remained low in the RAS, WHT, PEA and MIS residue treatments until the end of the incubation period, while net mineralization occurred in the other treatments, corresponding to a remineralization phase whose intensity depended on the residues (ALF > PEA > RAS ~ MIS). Within the nonamended 4–8 cm depth layer, the soil NO_3^- dynamics differed significantly between treatments, indicating that the above amended layer had an influence; i.e., NO_3^- accumulation was very large in the POT-GRI treatment, while a decrease was observed in the other treatments. Similar to the findings within the 0–4 cm layer, net immobilization followed by remineralization occurred (for the MUS, RC and SUB residue treatments), and remineralization was not observed for the PEA, ALF, WHT, RAS or MIS residues (Fig. 2d).

NH_4^+-N always remained low in the control soils (between 0.3 and 0.6 kg NH_4^+-N ha^{-1}) in both the GRI and SLU soils, with mean rates of 0.02 ± 0.07 and 0.06 ± 0.01 kg NH_4^+-N ha^{-1} day^{-1}, respectively, which were positive in the GRI soil in the first and second incubations and negligible in the SLU soil (data not shown). Under the residue-amended treatment, temporary accumulation of NH_4^+ was observed within the 0–4 cm layer on day 7 in the RC-SLU and MUS-GRI treatments, the contents of which reached 10.4 ± 2.0 and 8.0 ± 0.7 kg NH_4^+-N ha^{-1}, respectively (Fig. 2e). All the other treatments caused a decrease in the soil NH_4^+ content, but the contents were significantly ($P < 0.05$) higher in the SUB-GRI and RC-GRI treatments than in the other treatments. Within the 4–8 cm layer, the NH_4^+ increased slightly under the MUS, POT and RC residue treatments in both soils, while it remained very low under the other treatments (Fig. 2d). Considering the overall NO_3^- and NH_4^+ dynamics in the soil cores, i.e., mixing together the two-layer mineral N contents, similar dynamics were expressed per unit surface, but the total decrease in NO_3^- under most treatments was not detected, as in the top-layer dynamics (Fig 3a).

3.4. N_2O emissions

For the C-CO_2 emitted, the N_2O fluxes differed significantly between residue treatments, and high rates occurred immediately beginning at the start of the incubation (Fig. 3a, b). The MUS-GRI, RC-SLU and, to a lesser extent, SUB-GRI residue treatments presented high rates of N_2O emissions during the first 2 days of incubation. These rates then decreased dramatically, with the exception of that of the MUS-GRI residue treatment on day 4. The N_2O emissions occurred mostly within the first 10 days (between 67 and 94%), except for the WHT, MIS, PEA and RAS residues incubated in the GRI soil, which resulted in low net N_2O emissions throughout the incubation period. TheN_2O emission rates returned to those of the control after approximately 20 days for the ALF, MUS, and RC residues and after 40 days for the SUB residue. Therefore, the pattern of cumulative N_2O emissions strongly distinguished the different residues, with high total net emissions for the MUS-GRI (4828 ± 892 g N-N_2O ha^{-1}) treatment and intermediate emissions for the SUB-GRI (2818 ± 314 g N-N_2O ha^{-1}) and RC-SLU (2567 ± 1245 g N-N_2O ha^{-1}) treatments, while all the emissions of the other treatments were much lower and were not significantly different (<200 g N-N_2O ha^{-1}) (Fig. 3c).

The mean N_2O emission rates from the control soils were not significantly different for the GRI soil in the first and second incubations (equal to 0.4 ± 0.8 g N-N_2O ha^{-1} day^{-1}) but were significantly lower than the mean emission rate of the SLU soil (4.1 ± 3.7 g N-N_2O ha^{-1} day^{-1}) (Fig. S1, SM). The cumulative emissions during the 0- to 60-day incubation period were 19 ± 23 and 14 ± 3 g N-N_2O ha^{-1} for the GRI soil in the first and second incubations, respectively, and 167 ± 83 g N-N_2O ha^{-1} for the SLU soil. The cumulative emissions at the end of the incubation were not significantly different from those of the control for the RAS or WHT residue.

As a function of residue N added, the median *EF*-N_2O value was 0.78% of residue N emitted as N_2O in this dataset (Fig. 4). Seven out of the 12 treatments (ALF-SLU, RC-SLU, ALF-GRI, MUS-GRI, RC-GRI, MIS-GRI, and SUB-GRI) had an *EF*-N_2O > 0.6% (value proposed by the IPCC methodology). The *EF*-N_2O values were significantly higher ($P<0.05$) when incubated in SLU soil than when incubated in GRI soil for both ALF and RC residues. The *EF*-N_2O values of all the other residues were below or close to the IPCC *EF*-N_2O default value.

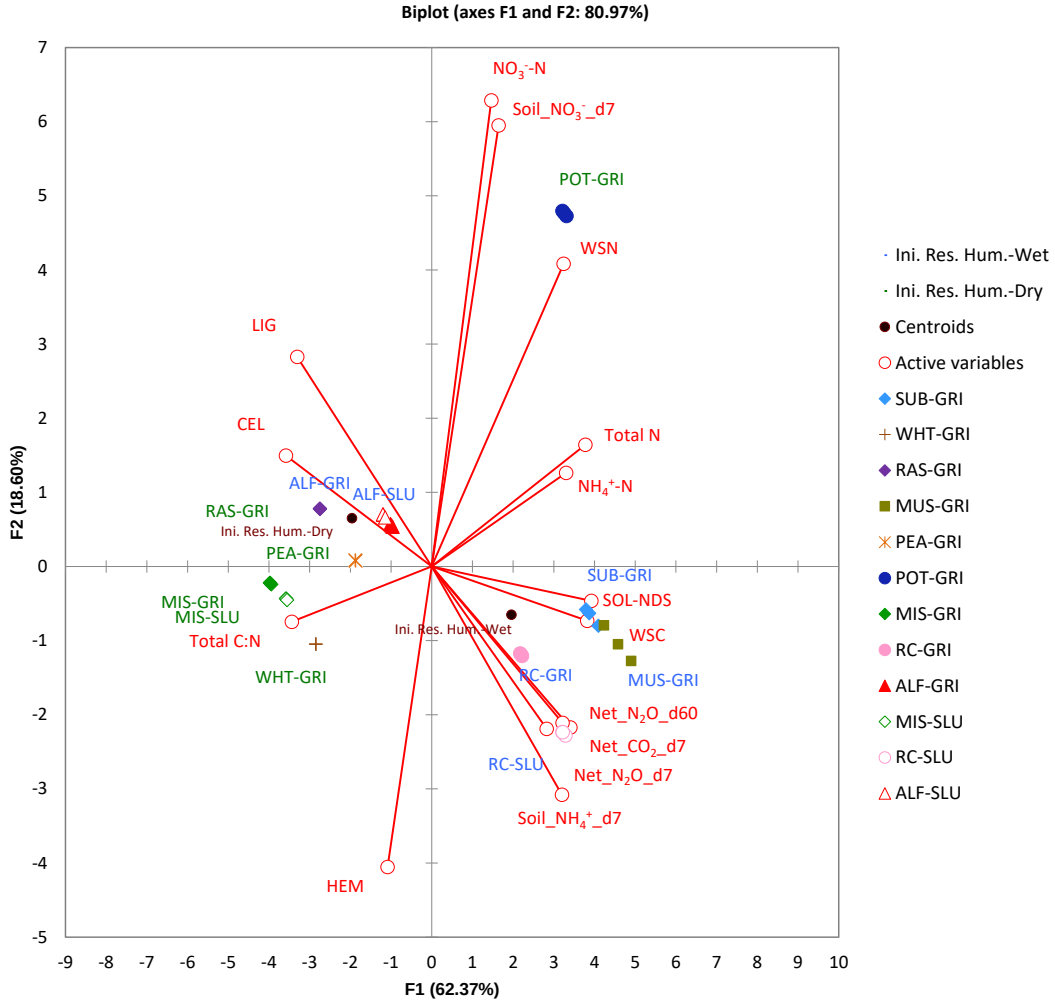

Figure 5. PCA of the initial residue chemistry, soil mineral N content, net CO_2 and N_2O emissions after 7 days of incubation, and net N_2O emissions after 60 days. The initial residue moisture class was used as an illustrative variable and was not taken into account in the PCA axis construction.

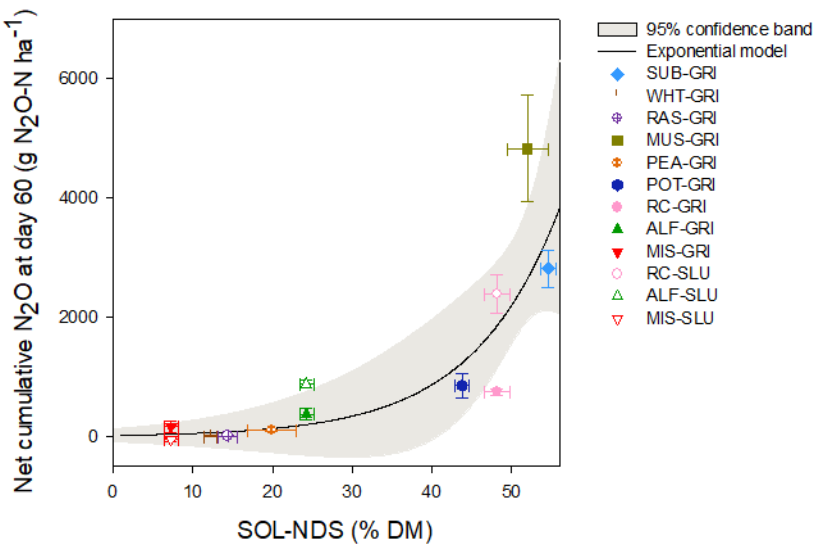

Figure 6. Relationships between observed and simulated net cumulative N_2O emissions on day 60, $netN2O_{d60}$, and residue SOL-NDS content. The symbols represent observed values (means ± SEs), and the line depicts the exponential regression equation ($netN2O_{d60} = 23.497 \cdot e^{0.093 \cdot SOL-NDS}$, r^2 = 0.71, r^2_a=0.69, P<0.002, cf. Table S3C).

3.5. PCA of residue characteristics and CO_2 and N_2O emissions

Fig. 5 shows the projection on the plane defined by the first two components of the PCA of the variables, including the initial residue chemical composition, soil mineral N content, net respiration, N_2O emissions after 7 days of incubation, net N_2O emissions after 60 days and *EF*-N_2O, as well as the observations of all residue-soil treatments. Axes 1 and 2 represent 62.4 and 18.6% of the total variance, respectively. Axis 1 was positively correlated with residue SOL-NDS content (r=0.99), WSC content (r=0.96), total N content (r=0.95), NH_4^+-N content (r=0.83), WSN content (r=0.82), net CO_2 respiration after 7 days of decay (r=0.86), NH_4^+-N content in the soil on day 7 (r=0.81), and net cumulative N_2O emissions on day 7 (r=0.71) and day 60 (r=0.81), all of which were associated with the MUS, SUB, RC and POT residue observations shown on the right-hand side of the plot. Axis 1 was negatively correlated with the residue CEL (r=-0.90), LIG (r=-0.89), and the total C:N ratio (r=-0.87), all of which were associated with the MIS, WHT, RAS, PEA, and ALF residue observations shown on the left-hand side of the plot. The residues were well distinguished according to this axis, showing high autocorrelation among chemical characteristics; the residue content in the SOL-NDS was also high in WSC content, total N content, NH_4^+-N content, and WSN content and low in CEL and LIG and had a low total C:N ratio. The centroid of the residue moisture classified as initially wet was projected on the right of axis 1, while the centroid of residue moisture classified as initially dry was projected on the left. Axis 2 was positively correlated with the NO_3^--N content of the residue (r=0.87), the soil NO_3^--N content on day 7 (r=82), and the WSN content (r=0.56), all of which were associated with the POT residue treatment at the top of the plot. Axis 2 was weakly negatively correlated with HEM (r=-0.56) and the soil NH_4^+-N content on day 7 (r=-0.42), which was mainly associated with the RC-SLU treatment at the bottom of the plot. AHC based on PCA partitioned the observations into 4 clusters, separating the treatments as follows: the MUS, SUB, and RC residues compose cluster 1; the POT residue composes cluster 2; the RAS, PEA, and AFL residues compose cluster 3; and, finally, the MIS and WHT residues compose cluster 4.

3.6. Distinguishing initial residue characteristics to predict N_2O emissions

All linear relationships between the net cumulative N_2O emissions on day 60 were used as independent variables, and the initial residue characteristics were used as dependent variables. A comparison between the best subsets of dependent variables in the models including one to all variables showed that the residue content in the SOL-NDS was clearly the best predictor of N_2O emissions from this dataset, as this variable was selected for inclusion into all the models (Table S3A). The regression model with the lowest Mallow C_P values and best r^2_a included the following 5 variables: residue SOL-NDS content, WSN content, and total C:N ratio, which had positive coefficients, and residue WSC and NO_3^--N contents, which had negative coefficients (Table S3B, r^2=0.72, r^2_a=0.74). The addition of other dependent variables did not significantly improve the regression prediction. The best nonlinear relationships were obtained via an exponential equation that included the SOL-NDS as the dependent variable with two coefficients (Fig. 6, Table S3C, r^2=0.72, r^2_a= 0.69), and the relationships including all the other variables were less predictive (r^2<0.5). The residual variability of the exponential regression with the SOL-NDS could not be significantly additionally explained by a second variable. Moreover, the goodness of fit of this exponential regression was very similar to that of the linear regression and had the advantage of including only one predictor.

3. Discussion

4.1 Coupling of decomposition dynamics and availability of soil mineral N

The nine crop species selected *a priori* on the basis of their differences in botanical family membership and agricultural use offered a group of residues with a gradual variation in biodegradability (Table 1, Fig. 1). The dynamics of decomposition in the soil revealed by the respiratory fluxes (Fig. 2) were slow for the most recalcitrant residue (MIS), for which the peak microbial activity occurred after 2 weeks, intermediate for residues that induced maximal respiration after 1 week (RAS, PEA, and WHT), and fast for the most labile residues (RC, MUS, SUB, POT, and ALF), for which the highest microbial activity occurred immediately from the beginning. These results confirm the findings of the large number of studies showing the relationships between the initial chemical characteristics of plant residues (so-called residue quality) and their biodegradability (Jensen

et al., 2005; Redin et al., 2014). The contrasting biodegradation dynamics observed in relation to the initial residue characteristics have crucial consequences for both the rate and the intensity of heterotrophic microbial growth and, therefore, the associated instantaneous oxygen demand, as well as the possible release of soluble C and soluble N compounds in the soil prior to microbial assimilation (Coppens et al., 2006; Surey et al. 2020). Together, all these factors are recognized as proximal drivers of N_2O emissions (Butterbach-Bahl et al., 2013).

The decomposition of crop residues with varying initial compositions influenced the amount, chemical form and distribution in the two layers of the soil columns of mineral N, the N substrate for microbial processes involved in N_2O production (Fig. 2). The NO_3^- dynamics exhibited a classic pattern associated with crop residue decomposition in the amended layer, i.e., an initial phase involving strong microbial immobilization until full depletion of mineral N was observed for several residues (Trinsoutrot et al., 2000). For the RC and PEA residues, the full depletion phase was followed by a second phase during which the NO_3^- content increased again, corresponding to the recycling of N with microbial death. The consumption of NO_3^- also occurred within the bottom 4–8 cm layer even when it was free of residues. First, the microbial activity leading to N immobilization may have involved soluble compounds that diffused from the top layer. Second, depletion could have occurred from the diffusion of NO_3^- from the bottom layer to the top layer according to the NO_3^- gradient caused by the high microbial consumption in the top layer. Usually, the residue-derived NH_4^+ that originates from decomposition does not accumulate significantly in soils because of the fast NH_4^+ consumption by either microbial immobilization or nitrification from decomposers colonizing the residue particles (de Ruijter et al., 2010). However, in this study, the MUS-GRI and RC-SLU treatments clearly exhibited peaks in NH_4^+ but did so transiently on day 3 before decreasing. For the two situations, this pattern suggests that the size of the protein N pool was high and that the early release of NH_4^+ linked to decomposition was greater than the NH_4^+ consumption; afterward, the trend reversed with the exhaustion of labile organic N. With the other labile residues (RC, SUB, and POT), NH_4^+ accumulation was much lower but remained significantly higher than that in the control soil during the first 10 days.

These higher soil NH_4^+ contents were related to CO_2- and N_2O-emitting situations, as reflected by the strong correlation between these variables according to the PCA, confirming the probable contribution of both nitrification and denitrification to N_2O production, particularly when oxygen becomes limiting or conditions are microanaerobic (Butterbach-Bahl et al., 2013). Such conditions certainly predominated in this study in the early stages of the decomposition of labile residues, which presented the highest N_2O emissions, and the initial CO_2 peak reflected microbial hotspots where the local available oxygen was fully consumed (Kravchenko et al., 2017). For the SUB and MUS residues, we determined that the volume of dioxygen (O_2) available in the residue-amended soil layer was approximately 5% of the requirements needed during the first 3 days based on the measured CO_2 emissions, which means that the O_2 supply was controlled by diffusion into the soil. The system may have been temporarily partially anoxic at the beginning of the incubation period with easily decomposable residues. This process was short-lived, most likely because, afterward, either the conditions became sufficiently oxygenated again, thus limiting N_2O production, or the N_2O produced was reduced to N_2. The water content during the incubations was equal to a WFPS of 60% in a zone where conditions are predominantly aerobic but can become anaerobic in certain spots; this is especially true for sandy loam-textured SLU soil, resulting in a water retention capacity that is lower than that of clay-textured GRI soil (Davidson et al., 2000). For the soil water content during the incubation, the soil ψ of the SLU soil was lower than that of the GRI soil, meaning that the water retention forces of the SLU soil particles were lower than those of the GRI soil particles; thus, compared with the GRI soil, the SLU soil probably contained more gravimetric water within the macropores and was closer to saturation. The relatively large proportion of saturated soil pores in the SLU soil compared with the GRI soil may have promoted oxygen limitation and N_2O formation in local areas, particularly through denitrification, inducing emissions that are higher than those from nitrification (Vilain et al., 2014). In addition, according to the study of Henault et al. (2019), the pH, CEC, and clay content of the SLU soil were within the ranges for which the reduction of N_2O to N_2 was not possible or nearly not possible, most likely because the reduction path was inhibited when the pH was lower than 6.8, as was the case in the SLU soil. These authors proposed two empirical indicators, both of which were measured in the laboratory, i.e., r_{max}, the

maximum ratio of accumulated N_2O to denitrified NO_3^-, and the *index*, the product of r_{max} and the during for which N_2O continued to accumulate during denitrification. The r_{max} and *index* values were higher than 0.8 and 50, respectively, for the SLU soil. In contrast, the GRI soil was classified as able to reduce N_2O (the r_{max} and *index* values were lower than 0.4 and 30, respectively). Therefore, compared with the GRI soil, the SLU soil was likely to emit more N_2O when the same residue was applied, as was the case for the RC and ALF residues.

4.2. Effects of crop residue characteristics on N_2O emissions

The different crop residues largely differed in their chemical composition, their respective proportions of soluble components and cell wall components, and their soluble C and total N concentrations. The same amount of residue DM was added to the incubated soil samples (4 Mg DM ha^{-1}), so the residue total N content and C:N ratio provided direct information on the total N added in the incubations, which varied from 14 kg N ha^{-1} for the MIS residue to 134 kg N ha^{-1} for the POT residue. The residue C:N ratio has been used to assess potential N_2O emissions primarily because it indicates the balance between N mineralization and N immobilization during decomposition and, therefore, the net residue N available in the soil (Nicolardot et al., 2001; Kumar and Goh, 2003). It is often considered that the threshold value is near C:N= 30, with N_2O emissions promoted if the residue C:N ratio is < 30 (Chen et al. 2013, Zhang et al. 2015). This threshold was confirmed here, and the treatments with residues having a C:N ratio of < 30 (POT, RC, MUS, and SUB) presented the highest N_2O emissions. However, our results showed that, compared with other indicators of residue chemical composition, the residue total N content or its C:N ratio was not the best predictor of N_2O emissions (Table S3) nor the lignin:N ratio, as suggested by Chantigny et al. (2002). The main insight from our results is the strong exponential response of the cumulative N_2O emissions after 60 days as a function of the residue SOL-NDS content. These results underscore the nonlinear relationships between N_2O emissions and residue characteristics; this is contrary to the *EF*-N_2O calculation, which implies a linear relationship with added N. The exponential equation sorted the low N_2O-emitting residues with low SOL-NDS and high-emitting residues (POT, RC, MUS, SUB, and ALF) with a threshold SOL-NDS value near 25% DM. The SOL-NDS fraction includes soluble compounds measured in hot water and in a neutral detergent; this fraction corresponds mainly to nonstructural compounds of plant cells (Chen, 2014). According to the large litter database analyzed by Jensen et al. (2005), this fraction included the largest proportion of plant material N (84% total N on average) and comparatively less plant C (46% total C on average). The importance of the water-soluble fraction has already been noted (Millar and Baggs, 2005; Rummel et al., 2020; Surey et al., 2020), and it is included in the SOL-NDS fraction. However, the chemical nature and biodegradability of these soluble fractions are not homogeneous (Marschner and Kalbitz, 2003; Lashermes et al., 2014). The SOL-NDS fraction contains short-chain carbohydrates, which constitute the majority of proteins and lipids, as well as complex organic compounds, waxes, and cutin (Peltre et al., 2012), some of which are labile and directly assimilated by microorganisms. Other compounds require the action of microbial extracellular enzymes to be degraded into smaller and more assimilable compounds (Moorhead et al., 2012; Lashermes et al., 2016), but their solubility favors microbial uptake because these microbial mechanisms occur in aqueous environments (Marschner and Kalbitz, 2003). Our findings showed that when residues had a large SOL-NDS fraction, their decomposition created hotspots of microbial activity made possible by the immediate assimilation of labile compounds and the facilitated degradation of soluble compounds, all while being a significant reservoir of nitrogen. Moreover, this fraction promotes direct N_2O emissions by nitrification from NH_4^+ and by denitrification in the presence of NO_3^- and a C source in hotspots, as stated by Mitchell et al. (2013). While this fraction stands out in this study, notably, the SOL-NDS-rich residues were also rich in WSC compounds and NH_4^+ but contained small amounts of cellulose and lignin. The cellulose and lignin contents of plants decrease with decreasing plant maturity, while the soluble compound contents increase (Bertrand et al., 2009); then, the decomposition of residues from immature crops favors these hotspots. Moreover, at similar concentrations, the chemical composition of soluble compounds released from different residues may vary and cause differences in CO_2 and N_2O production (Surey et al., 2020).

Initial moisture was an important factor for N_2O emissions, as residues with an initial moisture content of 0.80% (RC, MUS, SUB, and ALF) emitted more than residues with an initial moisture content of 0.20%. However, a major exception occurred for POT, the shoots of which were dry at the time of harvest but the

residue of which presented the same amount of N_2O emissions as the wet RC and ALF residues. The initial moisture content of the residue was chosen to reproduce the moisture content of the residue as closely as possible at the time of its return to the soil under real agricultural conditions (Machet et al., 2017). Water sorption by the residues at the start of the experiment may have created direct microenvironmental conditions within the residue that promoted emissions, as shown by Kravchenko et al. (2017). Humidification may have also promoted the solubilization of organic compounds and increased the water-extractable organic C content (Surey et al., 2020).

The current recommended values for residue *EF*-N_2O in national inventories have been revised to 0.6% (0.1–1.1%) and 0.5% (0.0–1.1%) of residue N for wet and dry climates, respectively (IPCC, 2019). The median *EF*-N_2O calculated in this study under controlled conditions (0.78% of the residue N) was indeed close to the revised value proposed as reference used by the IPCC methodology. Notably, in our dataset, the *EF*-N_2O overestimated the emissions for senescent residues with a high C:N ratio (C:N >40) and low SOL-NDS content (<25% of DM) compared to those we measured. In contrast, for residues that were physiologically nonsenescent, i.e., mature or still green at the time of recycling, the *EF*-N2O strongly underestimated the measured emissions, such as for SUB and MUS residues or depended on the soil type in which they were decomposed, such as for RC and ALF residues. Although the background emissions due to repetitive residue addition could not be evaluated with the design of this study, these results suggest that the IPCC methodology for *EF*-N_2O can be refined to avoid significant biases in the estimates of N_2O emissions when nonsenescent residues are added to the soil.

4. Conclusion

This study investigated gaseous emissions during soil decomposition of crop residues under controlled conditions and made it possible to clarify the effects of the chemical characteristics of a range of residues and the coupling of N_2O emissions with the dynamics of C and N mineralization. The results showed for the first time that total net N_2O emissions can be explained by a single chemical characteristic of residues: the SOL-NDS content. The nonlinear response of N_2O emitted to soluble residue content was captured by an exponential equation, which represents the low N_2O emissions from senescent residues with low SOL-NDS contents and the high emissions from residues with high SOL-NDS contents, regardless of whether they are physiologically mature or still green when they are returned to the soil. Other residue characteristics, such as the C:N ratio, N content, water soluble C and N contents, and initial moisture content, were also correlated with the SOL-NDS content but were less explanatory. The results of this study also showed that since N_2O emissions occurred mainly in the very first days of decomposition and were related to the consumption of soluble compounds, microbial assimilation of mineral N (i.e., N immobilization) further limited the N_2O emitted. Under the N-limiting conditions of this study, the residue chemistry was found to greatly affect the residue emissions, and the N_2O emissions from the recycling of residues that have not yet reached senescence are likely underestimated. More studies under different soil, climate, and management conditions are needed to assess whether the broad generalizations and estimates given by the IPCC methodology would need revisions to consider the residue chemical quality and to objectively weigh the other benefits these residues could bestow upon C storage, NO_3^- retention, and erosion limitation by soil cover.

Acknowledgments

The authors thank Sylvie Millon, Pascal Thiébeau, Olivier Delfosse, and Rachid Benabdallah for their technical assistance and Hugues Clivot for his insights into the statistical analysis during this project. We thank the two reviewers for their constructive comments, which improved the manuscript.

Funding

This work was supported by the ERA-NET FACCE ERA-GAS in the frame of the “Improved Estimation and Mitigation of Nitrous Oxide Emissions and Soil Carbon Storage from Cop Residues (Residue Gas)” project. FACCE ERA-GAS has received funding from the European Union’s Horizon 2020 Research and Innovation Program under grant agreement No. 696356. The French funding grant number was ANR-17-EGAS-0003.

Authors' contributions

G. Lashermes: Conceptualization, methodology, investigation, data curation, formal analysis, visualization, funding acquisition, and writing-original draft preparation; S. Recous: Conceptualization, funding acquisition, and writing-original draft preparation; G. Alavoine: Methodology, resources, investigation, and data curation; B. Janz: data curation, formal analysis, visualization, and writing-reviewing and editing; K. Butterbach-Bahl: Conceptualization, methodology, funding acquisition, and writing-reviewing and editing; M. Ernfors: Conceptualization, methodology, funding acquisition, and writing-reviewing and editing; P. Laville: Conceptualization, methodology, resources, investigation, data curation, formal analysis, visualization, and funding.

ORCIDs of the author(s): Gwenaëlle Lashermes: https://orcid.org/0000-0002-8269-3562; Sylvie Recous: https://orcid.org/0000-0003-4845-7811; Gonzague Alavoine: https://orcid.org/0000-0001-5741-1087; Baldur Janz: https://orcid.org/0000-0002-4477-2462; Klaus Butterbach-Bahl: https://orcid.org/0000-0001-9499-6598; Maria Ernfors: https://orcid.org/0000-0003-4300-4178; Patricia Laville: https://orcid.org/0000-0001-5904-8488

Data availability statement

The data that support the findings of this study are available at Data INRAE, https://doi.org/10.15454/8ASYPC

References

AFNOR, 2004. Water quality - Determination of nitrogen - Determination of bound nitrogen (TN sub b), following oxidation to nitrogen oxides NF EN 12260.

Alavoine, G., Houlbert, J.-C., Nicolardot, B., 2008. Comparison of three methods to determine C decomposition of organic materials in soils under controlled conditions. Pedobiologia 52, 61-68. https://doi.org/10.1016/j.pedobi.2008.03.001

Alavoine, G., Nicolardot, B., 2002. Comparison of potentiometric titration, IR spectrophotometry and segmented micro-flow analysis to determine inorganic C in alkaline solutions. Anal. Bioanal. Chem. 374, 354-358. https://doi.org/10.1007/s00216-002-1460-2

Bertrand, I., Prevot, M., Chabbert, B., 2009. Soil decomposition of wheat internodes of different maturity stages: Relative impact of the soluble and structural fractions. Bioresource Technology 100, 155-163. https://doi.org/10.1016/j.biortech.2008.06.019

Butterbach-Bahl, K., Baggs, E.M., Dannenmann, M., Kiese, R., Zechmeister-Boltenstern, S., 2013. Nitrous oxide emissions from soils: how well do we understand the processes and their controls? Philosophical Transactions of the Royal Society B: Biological Sciences 368, 20130122. https://doi.org/10.1098/rstb.2013.0122

Chantigny, M.H., Angers, D.A., Rochette, P., 2002. Fate of carbon and nitrogen from animal manure and crop residues in wet and cold soils. Soil Biol. Biochem. 34, 509-517. https://doi.org/10.1016/S0038-0717(01)00209-7

Chen, H., 2014. Biotechnology of Lignocellulose: Theory and Practice. Chemical Industry Press, Beijing and Springer, Dodrechet. https://doi.org/10.1007/978-94-007-6898-7

Chen, H., Li, X., Hu, F., Shi, W., 2013. Soil nitrous oxide emissions following crop residue addition: a meta-analysis. Glob. Change Biol. 19, 2956-2964. https://doi.org/10.1111/gcb.12274

Coppens, F., Garnier, P., De Gryze, S., Merckx, R., Recous, S., 2006. Soil moisture, carbon and nitrogen dynamics following incorporation and surface application of labelled crop residues in soil columns. Eur. J. Soil Sci. 57, 894-905. https://doi.org/10.1111/j.1365-2389.2006.00783.x

Davidson, E.A., Keller, M., Erickson, H.E., Verchot, L.V., Veldkamp, E., 2000. Testing a Conceptual Model of Soil Emissions of Nitrous and Nitric Oxides: Using two functions based on soil nitrogen availability and soil water content, the hole-in-the-pipe model characterizes a large fraction of the observed variation of nitric oxide and nitrous oxide emissions from soils. BioScience 50, 667-680. https://doi.org/10.1641/0006-3568(2000)050[0667:TACMOS]2.0.CO;2

de Ruijter, F.J., Huijsmans, J.F.M., Rutgers, B., 2010. Ammonia volatilization from crop residues and frozen green manure crops. Atmos. Environ. 44, 3362-3368. https://doi.org/10.1016/j.atmosenv.2010.06.019

Deng, H., Sun, J., Liu, N., Wang, H., Yu, B., Li, J., 2017. Impact of H2O broadening effect on atmospheric CO and N2O detection near 4.57μm. J. Mol. Spectrosc. 331, 34-43. https://doi.org/10.1016/j.jms.2016.11.001

FAO, 2017. Soil Organic Carbon: the hidden potential. Food and Agriculture Organization of the United Nations, Rome,

Italy. FAO editor. ISBN 978-92-5-109681-9. http://www.fao.org/3/i6937e/i6937e.pdf

Goering H.K., Van Soest P.J., 1970. Forage Fiber Analysis (Apparatus, Reagents, Procedures and Some Applications). Agriculture Handbook n°379. US Government Printing Office, Washington, Jacket n° -367-598.

Harazono, Y., Iwata, H., Sakabe, A., Ueyama, M., Takahashi, K., Nagano, H., Nakai, T., Kosugi, Y., 2015. Effects of water vapor dilution on trace gas flux, and practical correction methods. J. Agric. Meteorol. 71, 65-76. https://doi.org/10.2480/agrmet.D-14-00003

Hénault, C., Bourennane, H., Ayzac, A., Ratié, C., Saby, N.P.A., Cohan, J.-P., Eglin, T., Gall, C.L., 2019. Management of soil pH promotes nitrous oxide reduction and thus mitigates soil emissions of this greenhouse gas. Sci. Rep. 9, 20182. https://doi.org/10.1038/s41598-019-56694-3

Hergoualc'h K., Akiyama H., Bernoux M., Chirinda N., del Prado A., Kasimir A., MacDonald J.D., Ogle S.M., Regina K., van der Weerden T.J., 2019. N2O emissions from managed soils, and CO2 emissions from lime and urea application. Refinement to the 2006 IPCC Guidelines for National Greenhouse Gas Inventories, Chapter 11. Intergovernmental Panel on Climate Change (IPCC) editor. ISBN 978-4-88788-232-4.

IPCC, 2019. Refinement to the 2006 IPCC Guidelines for National Greenhouse Gas Inventories. The Intergovernmental Panel on Climate Change. https://www.ipcc.ch/report/2019-refinement-to-the-2006-ipcc-guidelines-for-national-greenhouse-gas-inventories/

Jensen, L.S., Salo, T., Palmason, F., Breland, T.A., Henriksen, T.M., Stenberg, B., Pedersen, A., Lundström, C., Esala, M., 2005. Influence of biochemical quality on C and N mineralisation from a broad variety of plant materials in soil. Plant Soil 273, 307-326. https://doi.org/10.1007/s11104-004-8128-y

Kamphake, L.J., Hannah, S.A., Cohen, J.M., 1967. Automated analysis for nitrate by hydrazine reduction. Water Res. 1, 205-216. https://doi.org/10.1016/0043-1354(67)90011-5

Kravchenko, A.N., Toosi, E.R., Guber, A.K., Ostrom, N.E., Yu, J., Azeem, K., Rivers, M.L., Robertson, G.P., 2017. Hotspots of soil N2O emission enhanced through water absorption by plant residue. Nat. Geosci. 10. https://doi.org/496.10.1038/ngeo2963

Klute A., 1986. Water retention: laboratory methods. Methods of Soil Analysis. Part 1- Physics and Mineralogical methods. Eds Soil Sci. Soc. Am. J., Madison, A. Klute, 687-734.

Krom, M.D., 1980. Spectrophotometric determination of ammonia: a study of a modified Berthelot reaction using salicylate and dichloroisocyanurate. Analyst 105, 305-316. https://doi.org/10.1039/AN9800500305

Kumar, K., Goh, K.M., 2003. Nitrogen Release from Crop Residues and Organic Amendments as Affected by Biochemical Composition. Comm. Soil Sci. Plant Anal. 34, 2441-2460. https://doi.org/10.1081/CSS-120024778

Lashermes, G., Gainvors-Claisse, A., Recous, S., Bertrand, I., 2016. Enzymatic Strategies and Carbon Use Efficiency of a Litter-Decomposing Fungus Grown on Maize Leaves, Stems, and Roots. Front. Microbiol. 7. https://doi.org/10.3389/fmicb.2016.01315

Lashermes, G., Moorhead, D., Recous, S., Bertrand, I., 2014. Interacting Microbe and Litter Quality Controls on Litter Decomposition: A Modeling Analysis. PLoS One 9. https://doi.org/10.1371/journal.pone.0108769

Laville, P., Fanucci, O., Chandra, V., 2019. Integrated mesocosms for N2 O emissions and soil carbon storage assessments: validation and qualification of a new laboratory device: IMNOA," 2019 IEEE International Workshop on Metrology for Agriculture and Forestry (MetroAgriFor), pp. 30-34, https://doi.org/10.1109/MetroAgriFor.2019.8909257

Le Guillou, C., Angers, D.A., Leterme, P., Menasseri-Aubry, S., 2012. Changes during winter in water-stable aggregation due to crop residue quality. Soil Use Manag. 28, 590-595. https://doi.org/10.1111/j.1475-2743.2012.00427.x

Li, C., Frolking, S., Butterbach-Bahl, K., 2005. Carbon Sequestration in Arable Soils is Likely to Increase Nitrous Oxide Emissions, Offsetting Reductions in Climate Radiative Forcing. Clim. Change 72, 321-338. https://doi.org/10.1007/s10584-005-6791-5

Linn, D.M., Doran, J.W., 1984. Effect of Water-Filled Pore Space on Carbon Dioxide and Nitrous Oxide Production in Tilled and Nontilled Soils. Eds Soil Sci. Soc. Am. J. 48, 1267-1272. https://doi.org/10.2136/sssaj1984.03615995004800060013x

Lugato, E., Leip, A., Jones, A., 2018. Mitigation potential of soil carbon management overestimated by neglecting N2O emissions. Nat. Clim. Change 8, 219-223. https://doi.org/10.1038/s41558-018-0087-z

Machet, J.-M., Dubrulle, P., Damay, N., Duval, R., Julien, J.-L., Recous, S., 2017. A Dynamic Decision-Making Tool for Calculating the Optimal Rates of N Application for 40 Annual Crops While Minimising the Residual Level of Mineral N at Harvest. Agronomy 7, 73. https://doi.org/10.3390/agronomy7040073

Marschner, B., Kalbitz, K., 2003. Controls of bioavailability and biodegradability of dissolved organic matter in soils. Geoderma 113, 211-235. https://doi.org/10.1016/S0016-7061(02)00362-2

Mary, B., Recous, S., Darwis, D., Robin, D., 1996. Interactions between decomposition of plant residues and nitrogen cycling

in soil. Plant Soil 181, 71-82. https://doi.org/10.1007/BF00011294

Millar, N., Baggs, E.M., 2005. Relationships between N2O emissions and water-soluble C and N contents of agroforestry residues after their addition to soil. Soil Biol. Biochem. 37, 605-608. https://doi.org/10.1016/j.soilbio.2004.08.016

Minasny, B., Malone, B.P., McBratney, A.B., Angers, D.A., Arrouays, D., Chambers, A., Chaplot, V., Chen, Z.-S., Cheng, K., Das, B.S., Field, D.J., Gimona, A., Hedley, C.B., Hong, S.Y., Mandal, B., Marchant, B.P., Martin, M., McConkey, B.G., Mulder, V.L., O'Rourke, S., Richer-de-Forges, A.C., Odeh, I., Padarian, J., Paustian, K., Pan, G., Poggio, L., Savin, I., Stolbovoy, V., Stockmann, U., Sulaeman, Y., Tsui, C.-C., Vågen, T.-G., van Wesemael, B., Winowiecki, L., 2017. Soil carbon 4 per mille. Geoderma 292, 59-86. https://doi.org/10.1016/j.geoderma.2017.01.002

Mitchell, D.C., Castellano, M.J., Sawyer, J.E., Pantoja, J., 2013. Cover Crop Effects on Nitrous Oxide Emissions: Role of Mineralizable Carbon. Soil Sci. Soc. Am. J. 77, 1765-1773. https://doi.org/10.2136/sssaj2013.02.0074

Moorhead, D.L., Lashermes, G., Sinsabaugh, R.L., 2012. A theoretical model of C- and N-acquiring exoenzyme activities, which balances microbial demands during decomposition. Soil Biol. Biochem. 53, 133-141. https://doi.org/10.1016/j.soilbio.2012.05.011

Nicolardot, B., Recous, S., Mary, B., 2001. Simulation of C and N mineralisation during crop residue decomposition: A simple dynamic model based on the C:N ratio of the residues. Plant Soil 228, 83-103. https://doi.org/10.1023/a:1004813801728

Peltre, C., Christensen, B.T., Dragon, S., Icard, C., Katterer, T., Houot, S., 2012. RothC simulation of carbon accumulation in soil after repeated application of widely different organic amendments. Soil Biol. Biochem. 52, 49-60. https://doi.org/10.1016/j.soilbio.2012.03.023

Redin, M., Guenon, R., Recous, S., Schmatz, R., de Freitas, L.L., Aita, C., Giacomini, S.J., 2014. Carbon mineralization in soil of roots from twenty crop species, as affected by their chemical composition and botanical family. Plant Soil 378, 205-214. https://doi.org/10.1007/s11104-013-2021-5

Rummel, P.S., Pfeiffer, B., Pausch, J., Well, R., Schneider, D., Dittert, K., 2020. Maize root and shoot litter quality controls short-term CO2 and N2O emissions and bacterial community structure of arable soil. Biogeosciences 17, 1181-1198. https://doi.org/10.5194/bg-17-1181-2020

Schmatz, R., Recous, S., Adams Weiler, D., Elias Pilecco, G., Luiza Schu, A., Lago Giovelli, R., José Giacomini, S., 2020. How the mass and quality of wheat and vetch mulches affect drivers of soil N2O emissions. Geoderma 372, 114395. https://doi.org/10.1016/j.geoderma.2020.114395

Sterckeman, T., Ciesielski, H., 1991. Principaux facteurs influant sur la détermination de l'azote minéral des sols. In L'azote et le soufre des sols - Troisièmes journées de l'analyse de terre - Blois, Ed Frontières, Gif sur Yvette, France, pp. 101-121.

Surey, R., Schimpf, C.M., Sauheitl, L., Mueller, C.W., Rummel, P.S., Dittert, K., Kaiser, K., Böttcher, J., Mikutta, R., 2020. Potential denitrification stimulated by water-soluble organic carbon from plant residues during initial decomposition. Soil Biol. Biochem. 147, 107841. https://doi.org/10.1016/j.soilbio.2020.107841

Thiébeau, P., Jensen, L.S., Ferchaud, F., Recous, S., 2021. Biomass and chemical quality of crop residues from European areas, V1 ed. Portail Data INRAE. https://doi.org/10.15454/LBI3U7

Trinsoutrot, I., Recous, S., Bentz, B., Line`res, M., Cheneby, D., Nicolardot, B., 2000. Biochemical Quality of Crop Residues and Carbon and Nitrogen Mineralization Kinetics under Nonlimiting Nitrogen Conditions. 64, 918-926. https://doi.org/10.2136/sssaj2000.643918x

Verhoeven, K.J.F., Simonsen, K.L., McIntyre, L.M., 2005. Implementing false discovery rate control: increasing your power. Oikos 108, 643-647. https://doi.org/10.1111/j.0030-1299.2005.13727.x

Vilain, G., Garnier, J., Decuq, C., Lugnot, M., 2014. Nitrous oxide production from soil experiments: denitrification prevails over nitrification. Nutr. Cycling Agroecosyst. 98, 169 - 186. https://doi.org/10.1007/s10705-014-9604-2

Xia, L., Lam, S.K., Wolf, B., Kiese, R., Chen, D., Butterbach-Bahl, K., 2018. Trade-offs between soil carbon sequestration and reactive nitrogen losses under straw return in global agroecosystems. Glob. Change Biol. 24, 5919-5932. https://doi.org/10.1111/gcb.14466

Zhang, J., Müller, C., Cai, Z., 2015. Heterotrophic nitrification of organic N and its contribution to nitrous oxide emissions in soils. Soil Biol. Biochem. 84, 199-209. https://doi.org/10.1016/j.soilbio.2015.02.028

Zhao, Y., Zhang, J.-b., Müller, C., Cai, Z., 2018. Temporal variations of crop residue effects on soil N transformation depend on soil properties as well as residue qualities. Biol. Fertil. Soils 54, 659-669. https://doi.org/10.1007/s00374-018-1291-8

Supplementary material

Table S1. Main characteristics of the two soils used for residue incubations

Soil		GRI	SLU
Localization		Thiverval-Grignon, France	Åkarp, Sweden
Latitude/Longitude		48°50'58.5"N 1°56'04.3"E	55°39'58.5"N 13°06'57.1"E
Type		Calcareous silty clay loam	Sandy loam
FAO classification		Calcaric Cambisol	Eutric Cambisol
Clay (g kg^{-1} dry soil)		214	158
Silt (g kg^{-1} dry soil)		358	224
Sand (g kg^{-1} dry soil)		147	618
$CaCO_3$ (g kg^{-1} dry soil)		275	<0.1
Cation exchange capacity (cmol+ kg^{-1} dry soil)		13.6	10.5
pH_{H2O}		8.3	6.2
Organic C (g kg^{-1} dry soil)		18.4	15
Total N (g kg^{-1} dry soil)		1.79	1.49
C:N ratio		10.3	10.1
Moisture at	pF 4.2	128.3 ± 4.4	85.5 ± 2.1
(g H_2O kg^{-1} dry soil)	pF 3.5	160.7 ± 2.1	113.1 ± 1.0
	pF 2.9	211.8 ± 2.3	151.3 ± 2.8
	pF 2.7	230.6 ± 0.3	162.6 ± 1.0
	pF 2.5	253.8 ± 4.0	177.9 ± 2.8
	pF 2	336.1 ± 4.4	244.9 ± 7.7

pF 1.7	374.9 ± 11.5	269.4 ± 10.2
pF 1.1	405.9 ± 3.7	305.3 ± 9.9

Table S2. ANOVA results with the least mean square calculated for biochemical fractions and significant differences between crop residues (n=27, significance level P < 0.001, Benjamini and Hochberg correction for P-values).

	WSN	WSC	SOL-NDS	HEM	CEL	LIG
MIS	0.02 ^{f}	0.6 ^{g}	7.3 ^{g}	26.4 ^{ab}	45.3 ^{bc}	20.3 ^{a}
WHT	0.07 ^{ef}	1.6 ^{ef}	12.2 ^{f}	31.3 ^{ab}	44.2 ^{bc}	11.7 ^{cd}
RAS	0.09 ^{def}	1.4 ^{f}	14.4 ^{f}	10.5 ^{c}	55.3 ^{a}	19.2 ^{a}
PEA	0.13 ^{def}	2.3 ^{e}	20.0 ^{e}	15.4 ^{c}	46.6 ^{b}	17.8 ^{ab}
ALF	0.18 ^{de}	4.4 ^{d}	24.3 ^{d}	14.5 ^{c}	41.9 ^{c}	18.6 ^{a}
POT	0.67 ^{a}	6.8 ^{c}	43.8 ^{c}	12.3 ^{c}	30.1 ^{d}	13.1 ^{bc}
RC	0.22 ^{cd}	8.5 ^{a}	48.2 ^{b}	23.4 ^{b}	22.8 ^{e}	5.1 ^{e}
MUS	0.36 ^{bc}	7.8 ^{b}	52.0 ^{a}	13.0 ^{c}	27.1 ^{d}	7.4 ^{de}
SUB	0.39 ^{b}	9.2 ^{a}	54.6 ^{a}	21.7 ^{b}	16.1 ^{f}	7.1 ^{de}
F	20	214	380	17	108	17
Pr > F	2E-07	3E-16	5E-17	6E-07	1E-13	8E-07
Significant	< 0.0001	< 0.0001	< 0.0001	< 0.0001	< 0.0001	< 0.0001

The different superscripted letters indicate significant differences between particular species of residue (within rows) (Tukey's HSD test, α=0.05).

Table S3. Relationships between the net cumulative N_2O emissions on day 60 and the initial residue characteristics. A) Best subsets of dependent variables used to predict the independent variable of N_2O emissions with linear regression. B) Linear regression coefficients and associated SEs for the model including the subset of dependent variables in A). C) Nonlinear regression coefficients and associated SEs for the best model obtained. The goodness of fit of the regression equations was evaluated through the r^2 and r^2_a values to account for the number of independent variables.

A) Best subset variables for linear regression

Variable number	Mallow Cp	R^2	R^2_a	SOL-NDS	WSC	NO_3^--N	WSN	Total C:N	Total N	CEL	LIG	HEM	NH_4^+-N
1	17.1	0.60	0.58	*									
2	11.5	0.66	0.64	*					*				
3	4.5	0.73	0.71	*	*	*							
4	3.9	0.75	0.72	*	*	*	*						
5	**3.3**	**0.78**	**0.74**	*	*	*	*	*					
6	4.9	0.78	0.73	*	*	*	*	*		*			
7	6.1	0.79	0.73	*	*	*	*	*	*				*
8	7.6	0.79	0.73	*	*	*	*	*		*	*	*	
9	9.4	0.79	0.72	*	*	*	*	*	*	*	*	*	
10	11.0	0.79	0.71	*	*	*	*	*	*	*	*	*	*

B) Best linear regression

Variables in model #5 from A)	Coefficient	Standard Error	P	r^2	r^2_a
Constant	-2540.0	802.1	0.004	0.78	0.74
SOL-NDS	162.9	43.5	<0.001		
WSC	-558.7	226.8	0.02		
Total C:N	11.6	6.9	0.101		
NO_3^--N	-4942.8	1513.5	0.003		
WSN	5742.1	2630.5	0.037		

B) Nonlinear regression based on SOL-NDS

Constants in exponential model: a*exp(b*SOL-NDS)	Coefficient	Standard Error	P	r^2	r^2_a
a	23.497	47.613	0.632	0.72	0.69
b	0.093	0.039	0.040		

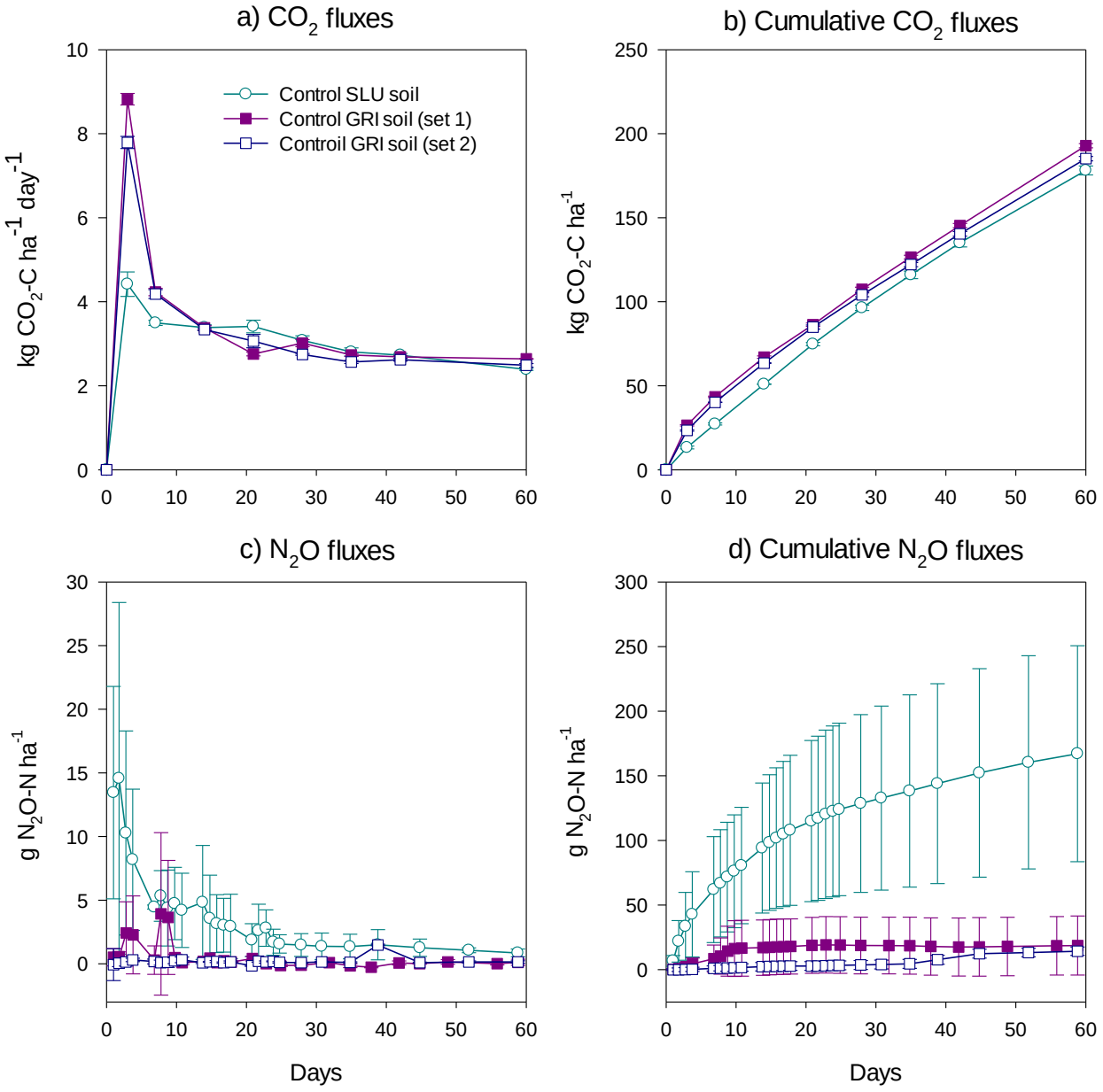

Figure S1. CO_2 and N_2O emissions from SLU and GRI control soils incubated at 15°C: a) CO_2 emission rates, b) cumulative CO_2 fluxes, c) N_2O emission rates, and d) cumulative N_2O fluxes.